Proc. of SPIE Vol. 2864, Optical System Contamination V, and Stray Light and System Optimization, ed. A M Glassford, R P Breault, S M Pompea (Nov 1996) Copyright SPIE

Flight measurement of contamination effects on fused silica mirrors

David F. Hall

The Aerospace Corporation
El Segundo, California 90245

ABSTRACT

A spacecraft was instrumented with five calorimeters and four temperature controlled quartz crystal microbalances. The calorimeters which are fitted with identical second surface silvered fused silica mirrors of the type frequently used for sun-illuminated spacecraft radiators, serve as contamination effects detectors. Two of the -50 °C TQCMs are located near four of the calorimeters. Over a four year period, the five calorimeter temperatures have increased because accumulated deposit of molecular contamination (from the outgassing spacecraft) has increased the solar absorptance of the mirrors. One, with a significant field of view of the spacecraft, has increased far more than the others which have either little or no spacecraft surfaces in their fields of view. The increases in calorimeter temperatures have been converted into increases in solar absorption. The ratios of these quantities range between 8×10^{-3} and 1.4×10^{-2} solar absorptance units per $\mu g/cm^2$ deposit. These values are consistent with industry practice of designing thermal systems with the expectation that sunlit surface solar absorptance will increase about 0.01 for every 100 Å of molecular contamination accumulated. Since the calorimeters were significantly warmer than the TQCMs, an even larger value of this ratio can be supported for conservative design of critical thermal systems.

2. INTRODUCTION

A program to measure spacecraft contamination in flight was described previously.[1] One of the spacecraft was instrumented with five calorimeters and four temperature controlled quartz crystal microbalances (TQCMs). Some of the data from the TQCMs were recently presented.[2]

The calorimeters have identical second surface silvered fused silica mirrors of the type frequently used for sun-illuminated spacecraft radiators as the samples. These mirrors have very nearly space stable solar absorptance values.[3,4] Therefore they make excellent "contamination effects" monitors, and it was for this purpose that the five calorimeters were placed in 3 locations on the spacecraft. Two of these locations are coincident with TQCMs, which measure the mass per unit area of molecular contamination as it accumulates on the sensing crystal.

As expected, the temperatures of the mirrors have been increasing with time and at different rates. The paper discusses the calibration of these instruments, the thermal model used to calculate the solar absorptances, and the correlation between these values and the quantity of contamination measured by the TQCMs.

These data will be useful to spacecraft thermal engineers who are often faced with the task of sizing sunlit radiators so they meet, but do not greatly exceed, end-of-mission thermal requirements. They will also be useful to spacecraft contamination modelers who need flight data to compare against their modeling assumptions. Of course, the ability to predict accurately the rate of molecular contamination build up and its effect on sensitive spacecraft surfaces (such as those of optical systems), is a powerful spacecraft and sensor design tool. Tools of this sort have been under development in the spacecraft contamination community for at least 25 years, but verifications, refinements, and extensions are still needed.

2. INSTRUMENTATION

2.1 Contamination Effects Monitor

In the present context, a calorimeter is any thermally isolated planar object in space, such as a thin disk or rectangular solid, fitted with a temperature sensor. Usually a thermal control coating is painted on, or a material is affixed to, one surface of

the disk. In this experiment, 5 fused silica mirrors, OCLI* SI-100, were the detectors. If a mirror bonded to the sample disk were perfectly isolated so that no heat entered its back surface or edges, and if it were normal to the sun-line, and if the temperature of space is negligible, in equilibrium the heat balance equation will be given by

$$Q\alpha_s A_D = \varepsilon_{hD}\sigma A_D T_D^4 \quad (1)$$

The quantity α_s is called the solar absorptance; it is the fraction of the incident sunlight absorbed by a solid. Another optical property of solids is the hemispherical infrared emittance, ε_{hD}. The subscript D has been added to denote the front surface of the detector. In Eq. 1, the Stefan-Boltzman constant is denoted σ, the detector temperature (in Kelvin units) T_D, the area of the exposed surface A_D, and the incident solar flux Q.

Real calorimeters do not have perfect thermal isolation. The disk must somehow be supported and its temperature sensed. Therefore, there will be heat conduction through the mechanical support(s) and the sensor wires if temperature differentials exist. In general, the disk will also have radiative heat interchange between its rear and edge surfaces and whatever is in line of sight of those surfaces. Furthermore, some solar energy enters the calorimeter through the few-mil-wide gap between the detector disk and its surrounding mount, and some of that is absorbed by the detector disk. Therefore Eq. 1 becomes more complicated:

$$Q\alpha_s A_D + \Delta Q_D = \varepsilon_{hD}\sigma A_D T_D^4 + \sum_i G_i\left(T_D - T_{Bi}\right) + \varepsilon_{hD}\sigma A_D \sum_i \beta_{Di}\left(T_D^4 - T_{Bi}^4\right) \quad (2)$$

Here ΔQ_D is the solar energy which enters the small gap around the detector and is absorbed by the disk, the G_i are heat conductance coefficients between the detector and its boundaries at temperatures T_{Bi}, the β_{Di} are radiant heat exchange coefficients, and the notation allows the emittance of the back and edge surfaces of the detector to be different than that of the front surface. The goal of calorimeter design is to make an instrument which is strong enough to withstand ground handling and launch, can survive the cold temperature of Earth eclipse, has negligible heat leaks, and little solar input through the gap. To date, the best design (Fig. 1) is due to Reichard and Triolo.[5,6] The heat leaks of this design are small enough to allow the flight data to be analyzed for changes in mirror solar absorptance, $\Delta\alpha_s$ under the assumption that all the heat leaks can be represented by a single conductance term between the detector and the bracket to which a calorimeter is mounted:

$$Q\alpha_s \equiv Q\left(\alpha_{s0} + \Delta\alpha_s\right) \cong \varepsilon_{hD}\sigma T_D^4 + \overline{G}\left(T_D - T_B\right) \quad (3)$$

Of course the value of $\overline{G}$ must have some dependence on T_D, as does ε_{nD}. The sensitivity of the detector is then given by

$$\frac{\partial\,\Delta\alpha_s}{\partial T_D} \cong 4\varepsilon_{hD}\frac{\sigma}{Q}T_D^3 + \frac{\sigma}{Q}T_D^4\frac{\partial\varepsilon_{hD}}{\partial T_D} + \frac{\overline{G}}{Q} + \frac{\partial\overline{G}}{\partial T_D}\left(\frac{T_D - T_B}{Q}\right) \quad (4)$$

Since these mirrors are space stable in the absence of contamination, any changes in the optical properties of the mirror surface will be due to contamination. The second term in Eq. 4 is negligible because the emissivity of fused silica is insensitive to temperature change over the temperature range encountered in sun-facing fused silica mirror calorimeters. Furthermore, ε_{hD} will not be much affected by a thin layer of contamination on the detector surface since the long wavelength internal reflectance and extinction coefficient of organic films are small. The third term in Eq. 4 is also small because the detector is insulated so well from the calorimeter bracket that the value of $\overline{G}$ changes slowly with T_D

2.2 Observables

All of the molecular contamination collected on spacecraft and sensor surfaces while on orbit originates from within the spacecraft materials of construction and from whatever the spacecraft carries to orbit on its surfaces. After a few hours of desorption, the molecules adsorbed on surfaces are largely depleted, and the contaminants released are predominated by molecules which slowly diffuse to the surfaces of solids and then escape. Because of the low ambient pressure of space, the mean free path of the molecules is much longer than the dimensions of the spacecraft, so with the possible exceptions of the plumes of thrusters and regions very near vents of the spacecraft interior volume, collisions between molecules are not significant.

* Optical Coatings Laboratory, Inc. Santa Rosa, California 95407-7397.

Figure 2 shows the classes of trajectories that released contamination molecules are known to take: line of sight (LOS), non line of sight (NLOS), and secondary surface (SS).[7] Figure 2 also depicts a spacecraft on which five calorimeters are mounted. Two pair are at the periphery of the despun platform, and each pair is separated by a TQCM. The calorimeters were paired for redundancy. The calorimeters of the pair with a completely clear field of view (FOV) of space are numbered 1 and 3, and they flank TQCM 1. They receive only NLOS molecules. The pair which have some secondary surfaces in their FOVs are numbered 2 and 4, and they flank TQCM 2. They receive NLOS, LOS, and SS molecules. Calorimeter 5 is mounted on an appendage and has some of the despun platform in its FOV. It likely receives about the same arrival rate of NLOS molecules, but a much higher rate of LOS and SS molecules than do calorimeters 2 and 4. Calorimeter 5 does not have an TQCM nearby because of engineering constraints.

Calorimeters 1 and 3 were expected to receive the least amount of contamination and calorimeter 5 the most because LOS transport is much more efficient than any of the NLOS transport forms.

2.3 Calibration

Although the calorimeters were calibrated at JPL[8] using a method originally described by Reichard and Triolo[9] the values obtained for calorimeter's heat leaks don't appear to be consistent with the orbital data. We intend to investigate this further. In the analysis presented here, the calorimeter detector and bracket temperature data have been used in a simple thermal model together with knowledge of the solar intensity and angle, and with the assumption that ε_{hD} is a constant. It was also necessary to assume the first orbital values of α_s and to extrapolate a first orbital value of each of the five calorimeter detector temperatures, T_{D0}, since spacecraft checkout and operations did not permit measurement of them. It can be shown that the increases in the solar absorptance, $\Delta\alpha_s$, are not very sensitive to these assumptions. Of course the absolute value of α_s is sensitive to the assumptions, especially the assumption of the value of α_{s0}.

The mirror solar absorptance to emittance ratios were assumed to be 0.09/0.8. The boundary temperatures of calorimeters 1-4 were assumed to be near that of their mounting brackets. (No temperature sensor reports calorimeter 5's mounting temperature, so it is assumed to be the average temperature of the brackets of the other calorimeters.) The radiant and conductive heat leaks and the gap solar flux absorbed by the detector were all lumped into $\overline{G}$ in Eq. 3, and its value calculated. This value of $\overline{G}$ was then used to convert measured values of values of T_D into $\Delta\alpha_s$ according to Eq. 3.

2.4 Measurement Procedure

During regular spacecraft use, the amount of solar illumination of the calorimeters on the spacecraft is a function of time. The procedure used to measure the calorimeter temperatures was to command the spacecraft to align and hold the calorimeters approximately normal to the sun-line while collecting data until the calorimeter temperatures appear to be nearing their equilibrium values. Even after two hours, final equilibrium was not reached, but by then there were enough temperature vs. time data to permit extrapolation to equilibrium. Because of the calorimeter locations on the spacecraft, three separate data collection periods were required: one for calorimeter 5, and one for each of the two pairs. With two exceptions (the first fall and the first spring measurements), the dates of the measurements were chosen such that the sun would be a few degrees below the despun platform. This minimized reflected and radiant heat loads on the sides and backs of the four platform-mounted calorimeters. The two exceptions resulted from problems in scheduling the measurements.

2.5 Data Analysis

To date, the analysis techniques utilized have been straightforward. Exponential curve fits have been made to some of the temperature vs. time data to obtain extrapolated equilibrium values, but usually we have just made use of the last value obtained after the approximate 2 hour equilibration time. The plots of equilibrium temperature vs. time presented in Section 3 are sufficient to give a qualitative understanding of the changes which occurred vs. time on orbit. Also shown are plots of $\Delta\alpha_s$ vs. time.

3. RESULTS

Figure 3 shows five years of equilibrium temperature data from the five calorimeters. The dashed lines are least squares linear fits to the data. As expected, the time rate of temperature increase of calorimeter 5 is the largest of the five, indicating it received contamination at a higher rate than did the other four calorimeters. It is somewhat puzzling that the absolute values of the other four calorimeter temperatures are as different as they are since they were built to be identical and similar amounts of contamination were expected to be deposited on them. In fact, the TQCMs near them measured a similar amount of contamination. A complication is that the spacecraft had been on orbit a significant length of time before the first calorimeter measurements were made. However, this cannot be the entire explanation because the five lines do not extrapolate backward in time to a single starting temperature. Neither do backward extrapolations of exponential fits to these data. Nor can the explanation be entirely due to location, since calorimeters 1 and 3 are paired but are a constant 3° C apart and calorimeters 2 and 4 are a nearly constant 1° C apart. The resolution of their measurements is 0.1° C, and it was expected that the accuracy would be ±0.2° C. Thus, either the calorimeters have different heat leak term magnitudes ($\overline{G}$ of Eq. 3), or the PRT temperature sensor system are not as accurate as expected (or both). Different heat leak magnitudes would result if some detector disks were left touching their surrounding annulus as a result of launch vibration. Nevertheless, these apparent problems are not major as long as the measurements are done about the same way each time and $\overline{G}$, whatever its value, is the same each time the measurement is made. As previously discussed, it is the change of temperature with time which is of greatest importance, since this change is produced by increasingly thick contamination deposits.

An interesting feature of all the calorimeter data is the "sawtooth" pattern wherein the temperature increases between fall and spring, while it decreases (to a lesser extent) between spring and fall. As shown in Figs. 4 - 8, when only the fall or only the spring data are considered, with the exception of the first to second fall measurement interval on calorimeters 2 and 4, both spring and fall data are monotonic with a slope not greatly different that that of the linear fit to all the data.

The sawtooth patterns of the fall to spring periods are believed to be a consequence of the biannual changes in the rate that contamination molecules leave the spacecraft interior. This process was discussed previously.[2] Peaks in rate occur near the spring and fall equinoxes when first one end and then the other end of the spacecraft are warmed by sunlight after they have spent 6 months in the dark condensing contamination molecules on their interior surfaces. The spring calorimeter temperature rate increase is larger than that of the fall, probably because (with the exceptions noted) the calorimeter measurements are made with the sun slightly below the despun shelf. Thus, in the spring, the measurement is taken *after* the sun begins to warm the aft end of the spacecraft and the contamination release rate is increased. In the fall, the measurement is taken *before* the sun begins to warm the forward end of the spacecraft. Apparently between the spring and the fall measurements some of these molecules are desorbed before encountering a VUV photon with sufficient energy to photolize them. That would explain the fact that fall readings were generally below those of the previous spring.

Since the unique first fall and the first spring measurements were taken with the sun above the platform, it is expected that the fall reading was increased over what would have been measured if it were measured while the sun was still below the platform. Conversely, since the first spring measurement was made before the sun began to heat the aft end of the spacecraft, it is expected that its measurement was decreased from what would have resulted had it been measured when the sun was below the platform. Inspection of figures 4-7 reveals that calorimeters 2 and 4 do have first temperatures warmer than can be extrapolated from the subsequent fall data. But a similar statement can also be made for the first spring data point. Furthermore, calorimeters 1 and 3 do not meet these expectations in either fall and spring, rather than what is proposed above. The reasons for all this is not known, but in any case, there is something clearly different about the first fall measurements of calorimeters 2 and 4.

The fact that calorimeters 2 and 4 have "anomalous" first fall data points makes comparison of their growth rates with those of calorimeters 1 and 3 difficult. These data make calorimeters 1 and 3 appear to have a temperature growth rate about twice that of 2 and 4, and the scatter of the 1 and 3 data about linear or exponential curve fits to the data much larger than that of the other three calorimeters. However, if the first fall data points of all calorimeters are ignored on the basis that the measurement timing was flawed, the resulting data set makes much more sense. For that data set, the temperature growth rate of calorimeters 1 through 4 are closer, and about 40% the calorimeter 5 growth rate.

Earlier it was noted that one expects calorimeters 1 and 3 (which have completely clear FOVs) to have a temperature growth rate which is less than that of 2 and 4 (which have part of a spacecraft appendage within their FOVs). Data from their respective -50 C TQCMs confirm that at the position of calorimeter 2 and 4 there is a higher deposition rate than at the position of 1 and 3, but only by about 10 %. Furthermore, it is not certain to what degree the TQCM data are directly comparable to that of the calorimeters since except when they are being measured, calorimeters 1-4 are maintained at much warmer temperatures (T > O °C, and usually around 20 °C) by heaters. These heaters prevent the calorimeters from dropping in temperature below the glass transition temperature of the adhesive used to bond the glass-frit-encased PRT to the back of the detector disk. Ground testing and earlier flights of similar units indicated that cracking the glass frit by differential contraction during cooling is a failure mode of these units. The heater on calorimeter 5 is not powered because no spare circuits were available at that location to provide the current. When shadowed for long periods, the calorimeters get much colder than -50 °C.

The next step is to convert the measured growth rates in temperatures into corresponding growth rates in solar absorptance of the mirrors. The method used was discussed in Section 2.3. The first fall data points were not used in performing the extrapolation to the launch date. The calculated values of $\Delta\alpha_s$ are presented in Fig. 9 It is seen that there is reasonable agreement between calorimeters 1 and 3 and between calorimeters 2 and 4, as one would expect. The surprise is that 2 and 4 apparently increase in solar absorptance less than 1 and 3 instead of more. This suggests that more sophisticated thermal modeling of the calorimeters may be warranted, and that is planned. As expected, calorimeter 5 increased the most, about 2.4 times as much as 1 and 3.

With the caveat concerning the difference in temperatures between calorimeter mirrors and TQCMs in mind, one may divide the accumulated $\Delta\alpha_s$ of each of the four calorimeters by the amount of accumulated mass per unit area measured by the adjacent TQCMs. Figure 9 also shows that calorimeters 1 and 3 have gained about 0.021 solar absorptance units in 4 years of fall data. TQCM 1, which is adjacent to these calorimeters has gained about 1.5 $\mu g/cm^2$ during this time. Dividing this into $\Delta\alpha_s$, one obtains 1.4×10^{-2} solar absorptance units per $\mu g/cm^2$ deposit ($\cong$0.014/100Å if the deposit has unity density). Figure 9 shows that calorimeters 2 and 4 have gained about 0.0145 solar absorptance units in 4 years. TQCM 2, which is adjacent to these calorimeters has gained about 1.7 $\mu g/cm^2$ during this time. Dividing this into $\Delta\alpha_s$, one obtains 8.6×10^{-3} solar absorptance units per $\mu g/cm^2$ deposit ($\cong$0.009/100Å if the deposit has unity density). These values are consistent with industry practice of designing thermal systems with the expectation that sunlit surface solar absorptance will increase about 0.01 for every 100 Å of molecular contamination accumulated. It is not understood why calorimeters 2 and 4 have a $\Delta\alpha_s$ to deposition ratio about 60% that of calorimeters 1 and 3. In any case, conservative radiator design should use a more pessimistic value, at least 1×10^{-2} per $\mu g/cm,^2$ in end-of-life performance estimates since the TQCMs would very likely have accumulated *less* contamination had they tracked the temperatures of calorimeters 1 through 4 throughout the period. That would lead to a *larger* effect to deposition ratio.

SUMMARY AND CONCLUSIONS

The measurements made with five calorimeters fitted with fused silica mirrors clearly show a significant effect of contamination build up with time. As expected, the calorimeter with the greatest area of the spacecraft within its FOV collected contamination at the highest rate. Over a 4 year period, its equilibrium temperature increased about 11 °C, corresponding to an increase in solar absorptance of 0.05. The calorimeters with a small amount of spacecraft surface within their FOVs increased in temperature about 2.6 °C, corresponding to increases in solar absorptance of 0.0145. The calorimeters with clear FOVs increased in temperature about 5.1 °C, corresponding to an increase in solar absorptance of about 0.021. The increases in solar absorptance of mirrors near the -50 °C TQCMs show that, at least for this vehicle's outgassing molecular spectrum (and considering the TQCMs are significantly colder than the mirrors), the ratio between change in solar absorptance and mass deposition is in the 8×10^{-3} to 1.4×10^{-2} solar absorptance units per $\mu g/cm^2$ deposit range. Since the calorimeters were significantly warmer than the TQCMs, an even larger value of this ratio can be supported for conservative design of critical thermal systems. The data are consistent with our understanding of deposition of relatively high vapor pressure molecules on surfaces as a two step process: condensation followed by photolization. Clearly spacecraft and instrument designers should pay special attention to surfaces which are sunlit some or all of the time, and whose optical

properties are important, especially if those surfaces have a line-of-sight relationship with a spacecraft vent or outgassing spacecraft material.

ACKNOWLEDGMENTS

This work was supported by the US Air Force Space Division under contract No. F04701-93-C-0094. The author wishes to thank Dick Parker and Roger Vought for assistance in collecting and processing the data, Bill Fischer and Roger Vought for assistance in thermal analysis, and Graham Arnold for helpful discussions.

REFERENCES

[1] D. F. Hall, "Spacecraft Contamination Flight Measurement Program," AIAA Preprint 87-1624, Presented to AIAA 22nd Thermophysics Conference, June, 1987.
[2] D.F. Hall, "Flight Measurement of Molecular Contaminant Deposition," Proc. of the SPIE, Vol. 2261, 1994.
[3] D. F. Hall and A. A. Fote, "Thermal Control Coatings Performance an Near Geosynchronous Altitude," *J. Thermophysics and Heat Transfer*, Vol. 6, No 4, pp. 665-671, Oct.-Dec. 1992.
[4] T. B. Stewart, G. S. Arnold, D. F. Hall, D. C. Marvin, W. C. Hwang, R. C. Young Owl, and H. D. Marten, "Photochemical Spacecraft Self-Contamination: Laboratory Results and Systems Impacts," *J. of Spacecraft and Rockets*, Vol. 26, No. 5, pp. 358-367, Sept-Oct., 1989.
[5] P. J. Reichard, and J. J. Triolo, "Preflight testing of the ATS-1 thermal coatings experiment," *Progress in Astronautics and Aeronautics*, Vol. 20, pp. 491-513, 1967.
[6] M. A. Brosmer, W. D. Fischer, and D. F. Hall, "Thermal Analysis of Flight Calorimeter Instrument Designs and Calibration Test Methods," AIAA Paper 87-1622, AIAA 22nd Thermophysics Conference, Honolulu, HI, June 1987.
[7] H. K. A. Kan, "Desorptive transfer: Mechanism of contaminant transfer in spacecraft," *J. Spacecraft*, Vol. 12 No. 1, pp. 62-64, Jan. 1975.
[8] J. Houseman and G. Siebes, "Calibration of calorimeter for measuring the performance of thermal control surfaces," *Materials in a Space Environment*, Centri National D'Etudes Spatiales, Toulouse, France, 1991, pp. 155-168.

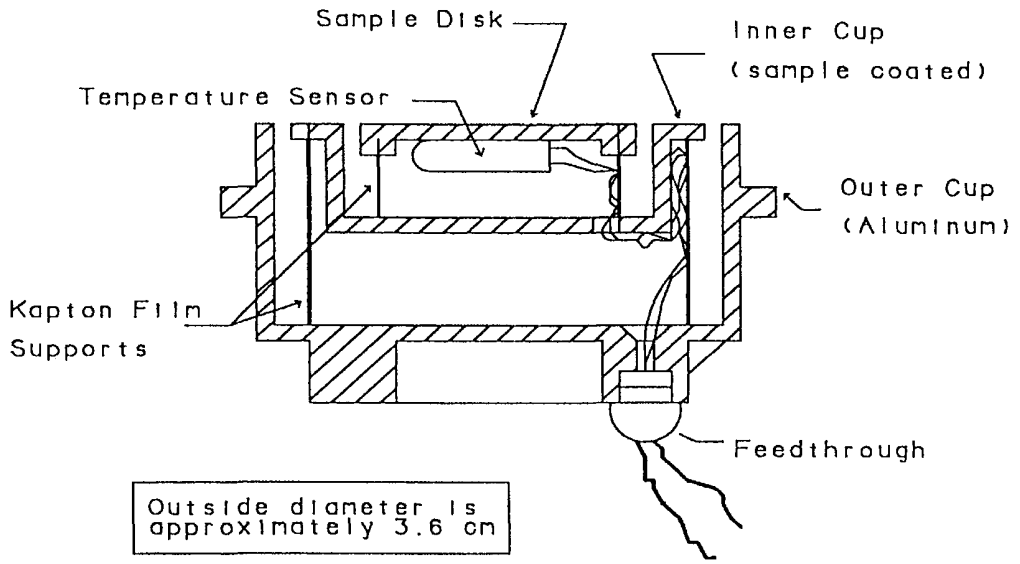

Fig. 1. Design features of the Reichard and Triolo[5] calorimeter.

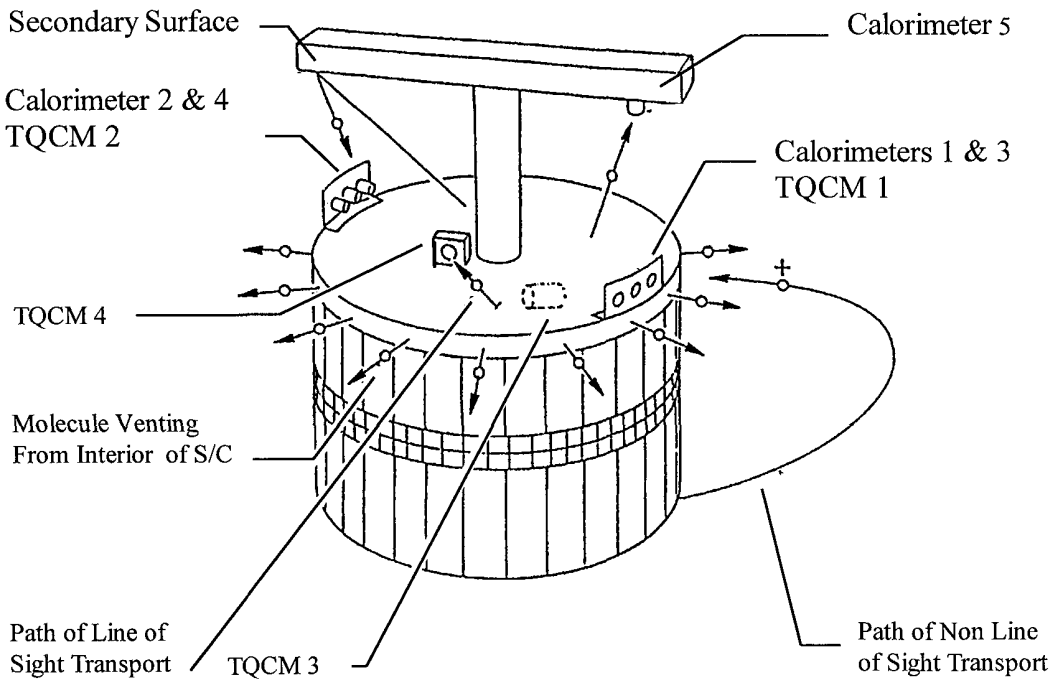

Fig 2. Calorimeter and TQCM locations on vehicle, and molecular trajectory classes.

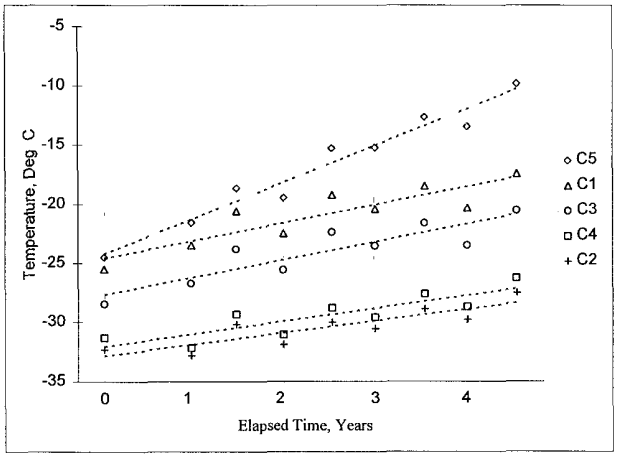

Fig. 3. Equilibrium calorimeter temperatures vs time.

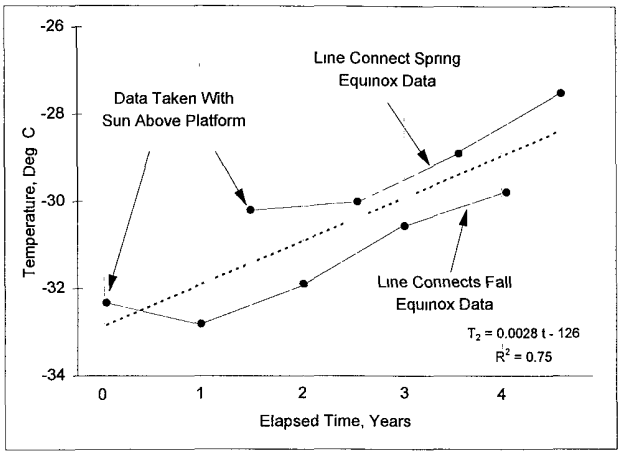

Fig. 6. Equilbrium temperature of calorimeter 2 vs. time.

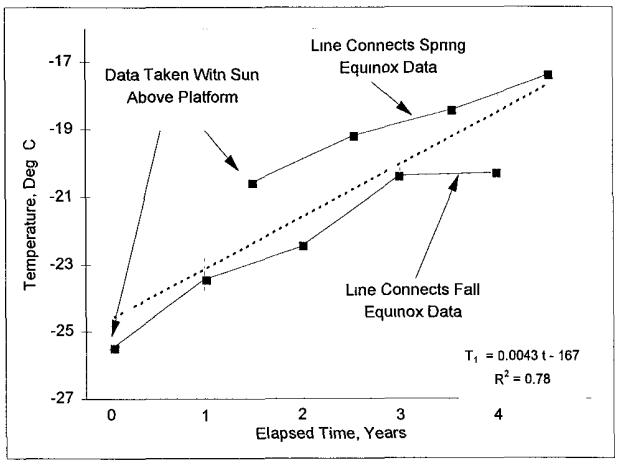

Fig. 4. Equilbrium temperature of calorimeter 1 vs. time.

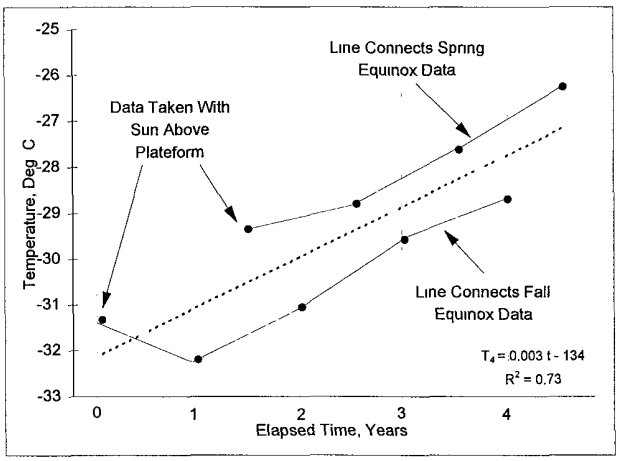

Fig. 7. Equilbrium temperature of calorimeter 4 vs. time.

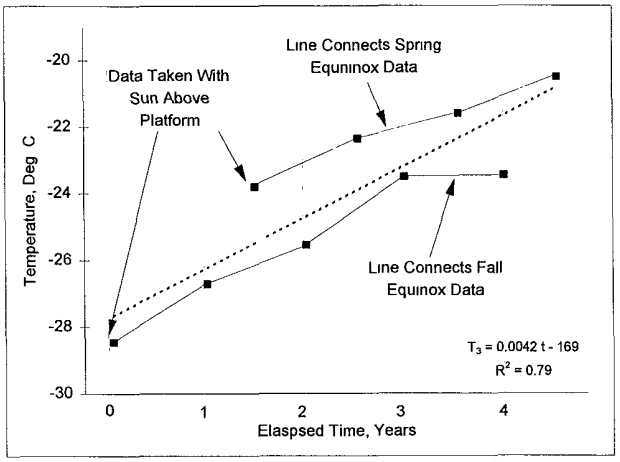

Fig. 5. Equilbruium temperature of calorimeter 3 vs. time.

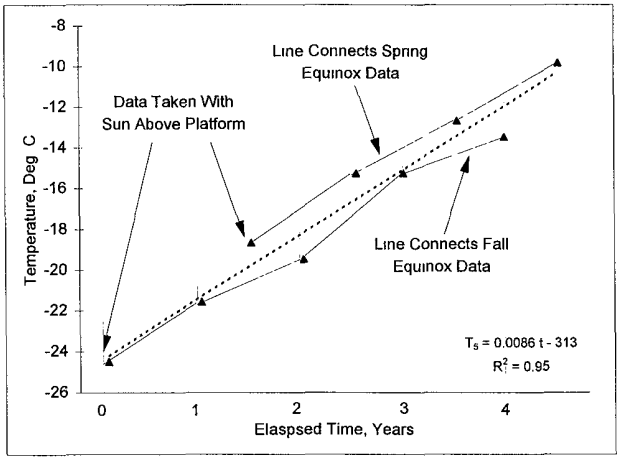

Fig. 8. Equilbruium temperature of calorimeter 5 vs. time.

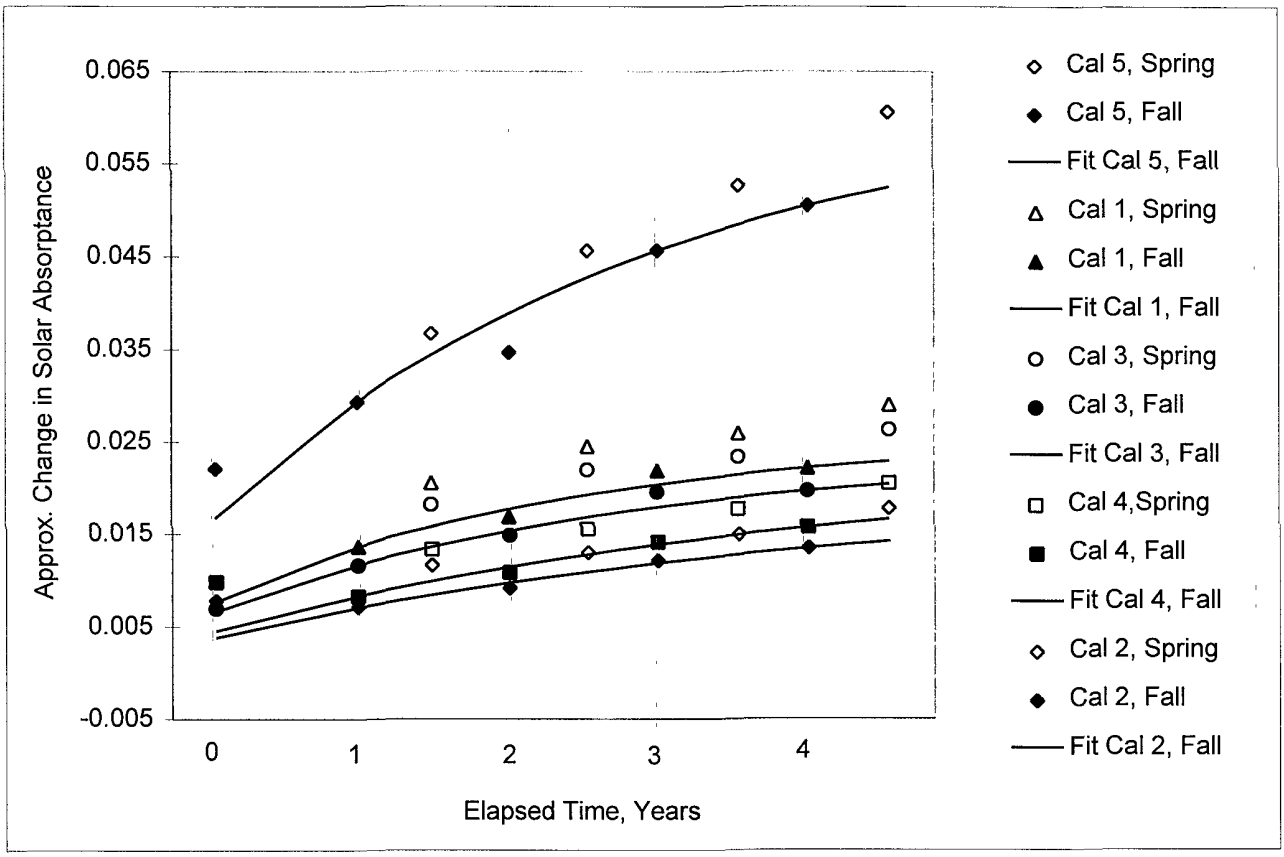

Fig. 9. Increases in mirror solar absorptances vs. time.